Volume 16
Number 6
23 March 2026
Pages 1891–2218

Catalysis Science & Technology

rsc.li/catalysis

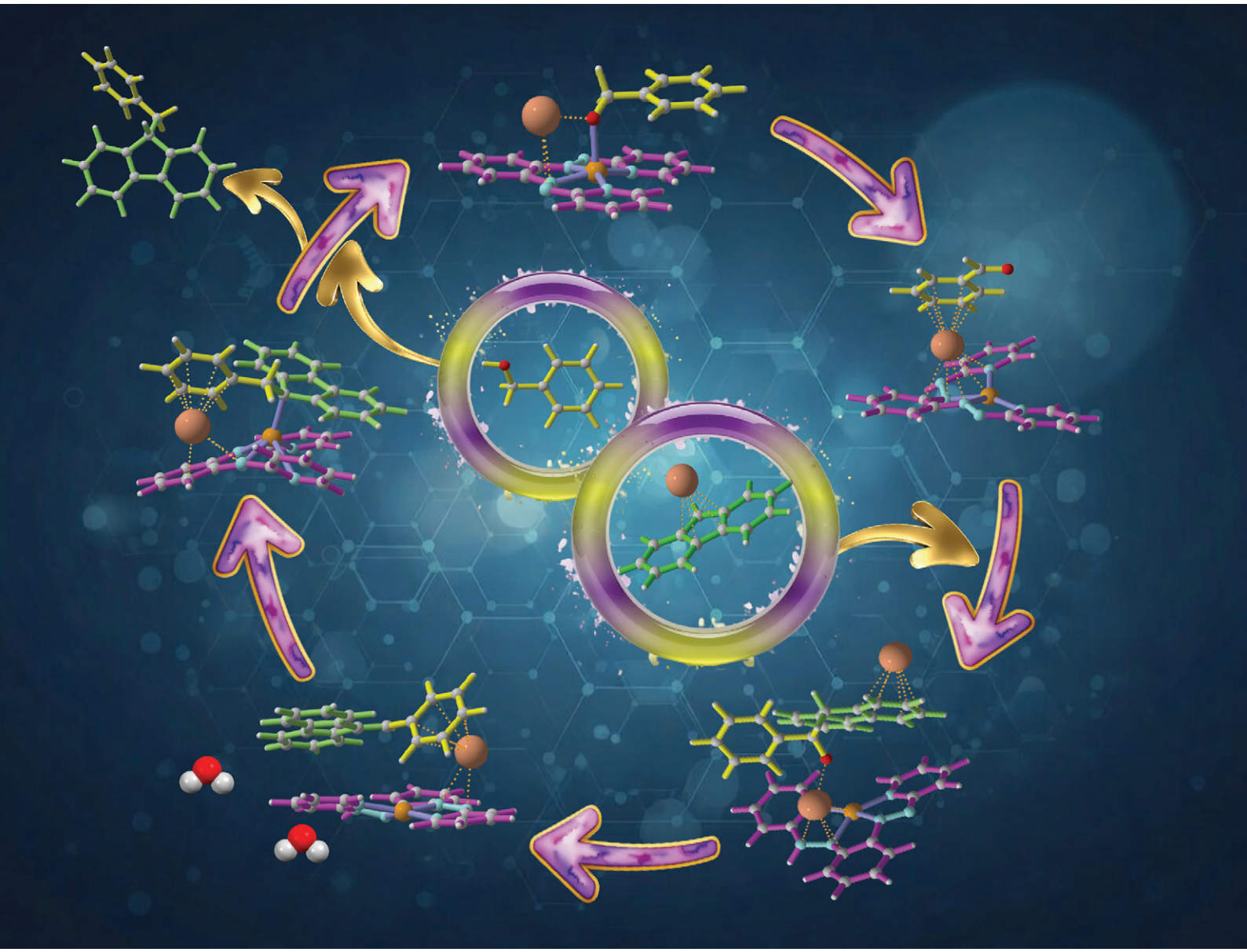

ISSN 2044-4761

ROYAL SOCIETY OF CHEMISTRY

PAPER

Avtar Changotra, Subhas Samanta *et al.*

sp^3 C–H alkylation of fluorenes catalyzed by *o*-phenylene-bridged noninnocent bis-azopyridyl complexes of copper

Catalysis Science & Technology

ROYAL SOCIETY OF CHEMISTRY

PAPER

View Article Online
View Journal | View Issue

Cite this: *Catal. Sci. Technol.*, 2026, **16**, 1935

sp^3 C–H alkylation of fluorenes catalyzed by *o*-phenylene-bridged noninnocent bis-azopyridyl complexes of copper

Kamal, †‡[a] Shivali Hans, ‡[a] Ambika Devi,[a] Nisha Yadav,[a] Muskan,[b] Avtar Changotra*[b] and Subhas Samanta *[a]

Received 5th August 2025,
Accepted 28th January 2026

DOI: 10.1039/d5cy00956a

rsc.li/catalysis

Herein, employing bio-inspired phenylene-bridged redox noninnocent bis-azopyridyl copper complexes, namely, [**1**]: [(L)$CuCl_2$] and [**2**]: [(L)CuCl], an efficient sp^3 C–H alkylation of fluorenes using alcohols as alkylating agents is reported, yielding alkylated fluorenes. Complex [**2**] was a better catalyst than complex [**1**]. The catalytic protocol employing [**2**] was very efficient and versatile across various fluorenes and benzyl alcohols. It also showed very good functional-group tolerance for both alcohols and fluorenes under lower base loadings and lower reaction temperatures. The protocol was also very effective in the synthesis of various fluorene-derived drug analogues of benflumetol. Mechanistic investigations by various spectroscopic techniques, control experiments, deuterium labelling studies, ^{1}H NMR kinetic analyses and DFT calculations revealed that a ligand radical–containing Cu(I) complex acted as the catalyst over the course of the reaction. Thus, complex [**2**] in the presence of KO^{t}Bu generated $K^+[(L)^{\bullet-}Cu^I(OCH_2Ph)]^{\bullet-}$ (**A**) as the active catalyst, in which the two redox noninnocent azopyridine moieties of the ligand participated in alcohol dehydrogenation, leading to the formation of the intermediate catalyst $K^+[(HL)^{2\bullet-}Cu^I(OCHPh)]^{\bullet-}$ (**B**). Subsequently, upon the reaction of **B** with the deprotonated fluorene, the electronically rich new intermediate **D** was formed, which facilitated the hydrogenation of the alkenylated fluorenes to yield alkylated fluorenes at comparatively lower temperatures.

Introduction

The development of new and efficient catalytic protocols for carbon–carbon and carbon–heteroatom bond-forming reactions using alcohols as reactants and 3d transition-metal complexes as catalyst(s) has received tremendous research interest in recent times.[1–6] This is because alcohols are sustainable, readily available, and environmentally benign feedstocks.[7–10] Moreover, 3d transition metals are affordable and earth-abundant.[5,6] Acceptorless dehydrogenation and borrowing hydrogen catalysis of alcohols have been emerged as prominent strategies in this aspect.[5,6] Commonly in these strategies, alcohols undergo dehydrogenation to generate carbonyl compounds by the transfer of proton and hydride to the metal complex. The carbonyl compound subsequently, *via* C–C and carbon–heteroatom bond formation reaction, forms an unsaturated intermediate compound.[5,6] This unsaturated intermediate compound retrieves a proton and a hydride from the catalyst intermediate, yielding the final product and regenerating the active catalyst.[5,6] In such a pathway, the hydrogenation step is often challenging and typically requires high temperature.[5,6] Recently, we, as well as others, have shown similar C–C and carbon–heteroatom bond formation reactions that occur in comparatively milder conditions using redox–noninnocent ligand–containing complexes.[11–13] However, investigations on the development of protocols that operate under more facile and milder reaction conditions are still ongoing.[14] It is worth noting that, though 3d complexes of Mn, Fe, Ni and Co have been successfully employed in these strategies,[15,16] such C–C bond formation reactions using Cu complexes remain scarcely reported to date,[16c] in spite of Cu being one of the most earth-abundant, affordable and sustainable metals. Moreover, it is observed that many biologically important metalloenzymes contain Cu at their active site(s), and these can act as catalysts in chemical transformations *via* the C–H bond activation reaction.[17–19] Galactose oxidase is a classic example that oxidizes alcohol under very mild reaction conditions.[20–22] The redox-active

[a] *Department of Chemistry, Indian Institute of Technology Jammu, Jagti, Jammu 181221, India. E-mail: subhas.samanta@iitjammu.ac.in*
[b] *Department of Chemistry, School of Sciences, Cluster University of Jammu, Canal Road, Jammu 180001, India*
† Current address: Institute for Chemical Research, Kyoto University, Gokasho, Uji 611-0011, Japan.
‡ Kamal and S. H. contributed equally to this manuscript and share first authorship.

tyrosine radical ligand coordinated with copper plays a key role in the rate-determining step of the α-CH activation of alcohol.[19a,c,21b] Thus, the development of efficient catalytic protocols using Cu-based complexes is highly important because of its sustainability and environmental friendliness. Herein, using a redox, noninnocent bis-azopyridyl copper complex [2], we report a highly efficient Cu(I)-based catalytic system for the sp^3 C–H alkylation of fluorenes under mild conditions (Scheme 1).

Recently, we reported redox noninnocent bis-azopyridyl copper complexes that were highly efficient and versatile for both aliphatic and aromatic alcohols.[23] The ligand-based redox events were solely involved over the course of the reaction. Moreover, we observed that a low-valent, electronically rich Cu(I) complex was involved during the catalytic reaction. Generally, such complexes are likely to be better reducing than their higher-valent complexes. Thus, we expected that complexes [1] and [2] (Scheme 2) would be beneficial in alcohol dehydrogenation–triggered C–C bond formation reactions. Accordingly, we were highly interested in exploring these complexes for the C–C bond formation reactions between fluorenes and alcohols. Indeed, both complexes [1] and [2] were highly efficient in this reaction. The complex [2] was a better pre-catalyst compared to [1]. Complex [2] (1.5 mol%), KO^{t}Bu (0.15 mmol), benzyl alcohol (1.5 mmol) and fluorene (1.0 mmol) were the optimized catalytic protocol for this reaction. This protocol demonstrated highly efficient and versatile (**59** examples, Scheme 1) catalytic activity with various fluorenes and alcohols. Notably, fluorenes are key starting materials for the synthesis of polyalkylated fluorenes, which exhibit interesting physical, chemical and electronic properties.[24,25] Moreover, functionalized fluorenes are highly important in pharmaceutical and materials applications (Scheme 1).[24–26] The catalytic protocol presented here was indeed very efficient in the synthesis of various fluorene-derived drug analogues of benflumetol. Currently, using alcohol as a reactant and transition metal complexes,[15,16] particularly 3d-metal complexes, as catalyst(s),[15b–e,g,16] such reactions are under

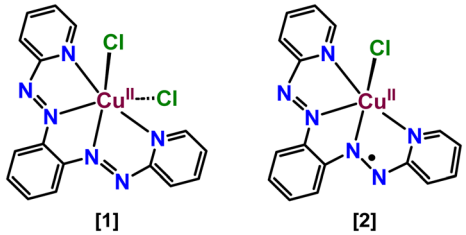

Scheme 2 Copper complexes [1] and [2] used in this study.

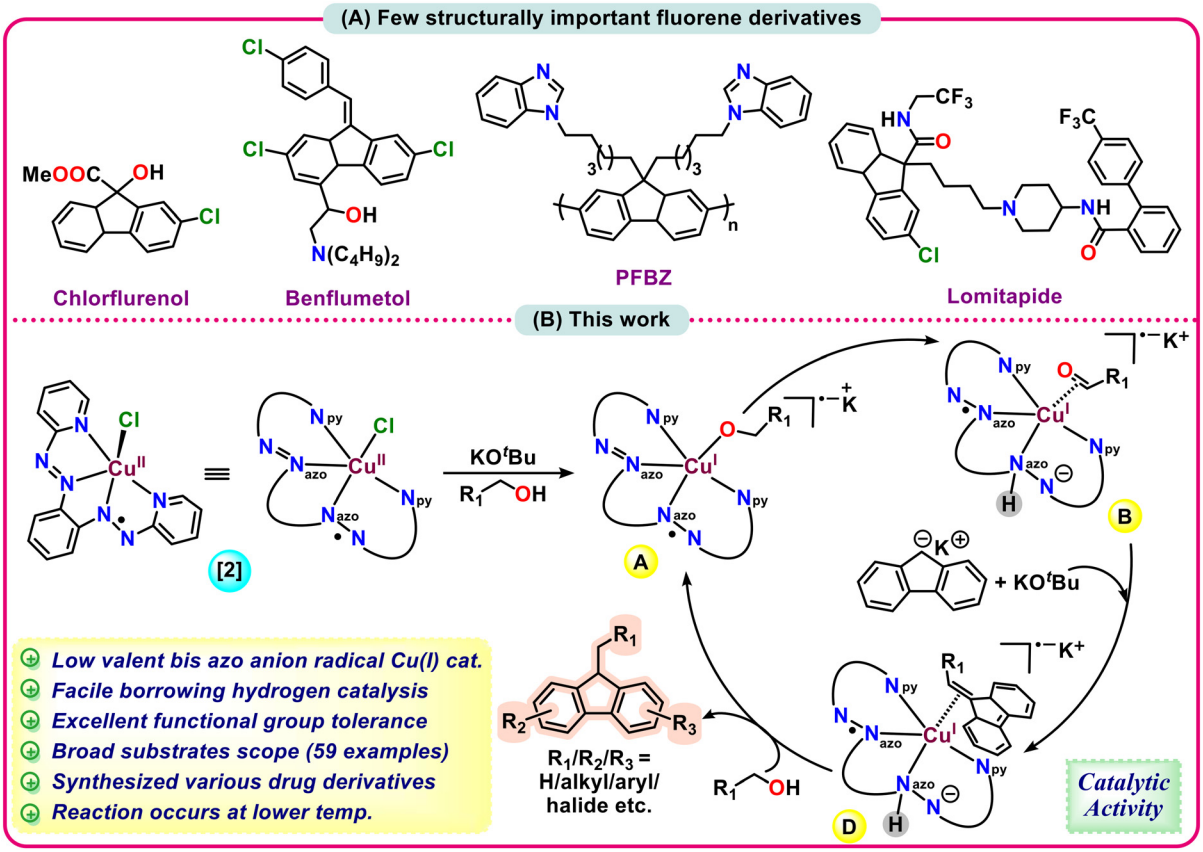

Scheme 1 Few structurally important fluorene derivatives (A) and complex [2] catalyzed C–C bond forming reactions in fluorenes (B).

exploration.[15d–f,16] Compared to the reported catalytic systems, the present system is found to operate at a lower temperature (Table S1). Mechanistic investigations showed that the complex [**2**] in presence of KO^{t}Bu generates $K^+[(\mathbf{L})^{\bullet-}Cu^I(OCH_2Ph)]^{\bullet-}$ (**A**) as the active catalyst, in which the two redox noninnocent azo-pyridyl motifs facilitate the dehydrogenation of alcohol (Scheme 1B), with the formation of intermediate catalyst $K^+[(\mathbf{HL})^{2\bullet-}Cu^I(OCHPh)]^{\bullet-}$ (**B**, Scheme 1). Subsequently, the C–C coupling reaction between the carbonyl compound in **B** and deprotonated fluorene generates the intermediate **D** (Scheme 1B), which, upon borrowing-hydrogen-type hydrogenation, results in the alkylated fluorene product. As the catalyst intermediate **D** contains low-valent Cu(I) metal and overall, it is electronically very rich (Scheme 1), the generally difficult hydrogenation reaction[27a,b] of the alkene intermediate of fluorene occurs successfully at lower temperatures. Thus, the redox, noninnocent bis-azopyridyl copper complex [**2**] is indeed very efficient under mild reaction conditions.

Results and discussion

The synthesis of the ligand [**L**] and its complexes [**1**] and [**2**] used in this work (Scheme S1) was reported by us very recently.[23] The catalytic sp^3 C–H alkylation of fluorenes using our synthesized bis-azopyridyl–derived copper complexes was commenced with the reaction of fluorene and benzyl alcohol. A combination of 1.0 mmol of fluorene, 1.5 mmol of benzyl alcohol, 0.15 mmol of KO^{t}Bu and 1.5 mol% pre-catalyst [**1**] indeed resulted in 9-benzyl-9*H*-fluorene, **5aa**, in 85% yield after 16 h in toluene at 90 °C (Table 1, entry 1). The catalytic efficiency of the pre-catalyst [**2**] was further evaluated under these reaction conditions, which showed that [**2**] was better than [**1**], and it provided 97% yield in 16 h (Table 1, entry 2). Thus, pre-catalyst [**2**] was used for further studies. Screening of solvents like DMF, acetonitrile, toluene, *o*-xylene, *p*-xylene, 1,4-dioxane showed that toluene was the best solvent for the reaction (Table 1, entries 3–7). Screening of bases like KO^{t}Bu, NaO^{t}Bu, NaOH, KOH, Cs_2CO_3, Na_2CO_3 and K_2CO_3 revealed that toluene in combination with KO^{t}Bu was the best

Table 1 Optimization of the C9-alkylation of fluorene with benzyl alcohol

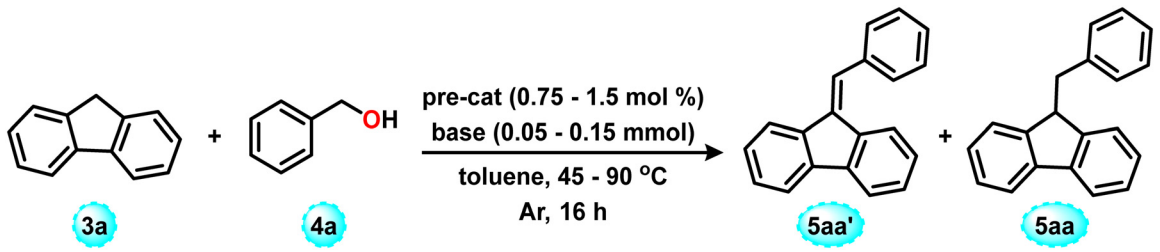

Entry	Pre-cat. (mol%)	Base (mmol)	Solvent	Temp (°C)	% yield (**5aa**)
1	[**1**] (1.5)	KO^{t}Bu (0.15)	Toluene	90	85
2	[**2**] (1.5)	KO^{t}Bu (0.15)	Toluene	90	97
3	[**2**] (1.5)	KO^{t}Bu (0.15)	DMF	90	17
4	[**2**] (1.5)	KO^{t}Bu (0.15)	Acetonitrile	90	15
5	[**2**] (1.5)	KO^{t}Bu (0.15)	*o*-Xylene	90	38
6	[**2**] (1.5)	KO^{t}Bu (0.15)	*p*-Xylene	90	40
7	[**2**] (1.5)	KO^{t}Bu (0.15)	1,4-Dioxane	90	32
8	[**2**] (1.5)	NaO^{t}Bu (0.15)	Toluene	90	70
9	[**2**] (1.5)	NaOH (0.15)	Toluene	90	36
10	[**2**] (1.5)	KOH (0.15)	Toluene	90	37
11	[**2**] (1.5)	Cs_2CO_3 (0.15)	Toluene	90	38
12	[**2**] (1.5)	Na_2CO_3 (0.15)	Toluene	90	15
13	[**2**] (1.5)	K_2CO_3 (0.15)	Toluene	90	18
14	[**2**] (1.5)	KO^{t}Bu (0.10)	Toluene	90	61
15	[**2**] (1.5)	KO^{t}Bu (0.05)	Toluene	90	41
16	[**2**] (1.0)	KO^{t}Bu (0.15)	Toluene	90	57
17	[**2**] (0.75)	KO^{t}Bu (0.15)	Toluene	90	36
18	[**L**] (1.5)	KO^{t}Bu (0.15)	Toluene	90	5
19	[**L**] (1.5) + **CuCl** (1.5)	KO^{t}Bu (0.15)	Toluene	90	12
20	—	KO^{t}Bu (0.15)	Toluene	90	4
21	[**1**] (1.5)	—	Toluene	90	n.r.
22	—	—	Toluene	90	n.r.
23	**CuCl** (1.5)	KO^{t}Bu (0.15)	Toluene	90	10
24[a]	[**2**] (1.5)	KO^{t}Bu (0.15)	Toluene	75	65
25[b]	[**2**] (1.5)	KO^{t}Bu (0.15)	Toluene	60	34
26[c]	[**2**] (1.5)	KO^{t}Bu (0.15)	Toluene	45	18

Reaction conditions: pre-cat. (0.75–1.5 mol%), fluorene (166.22 mg, 1.0 mmol, 1.0 equiv.), benzyl alcohol (162.2 mg, 1.5 mmol, 1.5 equiv.), base (0.05–0.15 mmol), solvent (3.0 mL, 0.33 M), 45–90 °C (oil bath), 16 h under an argon atmosphere. n.r. = no reaction. [a] Yield of **5aa′**: 8%. [b] Yield of **5aa′**: 40%. [c] Yield of **5aa′**: 36%. Yields were determined *via* ^{1}H NMR.

(Table 1, entries 8–13). Optimization of pre-catalyst and base loadings showed that 1.5 mol% pre-catalyst [**2**] along with 0.15 mmol of KO^{t}Bu afforded the best yield of product **5aa** (Table 1, entries 14–17). The reaction of fluorene with benzyl alcohol in the presence of base, along with free ligand [**L**], resulted in the alkylated product, **5aa**, in only 5% yield (Table 1, entry 18). A separate reaction involving base KO^{t}Bu, [**L**] and **CuCl** also resulted in the C9-alkylated product in 12% yield (Table 1, entry 19). Notably, using only KO^{t}Bu, product **5aa** was formed in just 4% yield (Table 1, entry 20). Here, it is pertinent to mention that no product was found to be formed in the absence of both KO^{t}Bu and pre-catalyst [**2**] (Table 1, entries 21 and 22). The metal salt precursor CuCl in combination with KO^{t}Bu resulted in only 10% of the desired product **5aa** (Table 1, entry 23). Further optimization of the temperature revealed that 90 °C was enough for the alkylation of fluorene (Table 1, entries 24–27). When we monitored the reaction under this condition at 90 °C with ^{1}H NMR, it was found that the rate of consumption of fluorene and the rate of formation of product **5aa** were almost the same (Fig. 1A). However, when we have examined the reaction at 75 °C, a significant amount of the intermediate **5aa′** was found to be accumulated in the reaction mixture (Fig. 1B and Table 1, entry 24). Furthermore, when the reaction was performed at 60 °C, it was found that the hydrogenation of intermediate **5aa′** was much slower, and the reaction produced a mixture of reactant, intermediate and product (Fig. 1C and Table 1, entry 25). Further reducing the temperature to 45 °C showed incomplete conversion, yielding a mixture of reactants and products **5aa** and **5aa′** (Table 1, entry 26). Thus, it indicated that the 90 °C is the optimal temperature, and once the alkene intermediate **5aa′** forms, it undergoes facile hydrogenation to result in product **5aa**. Thus, the optimized reaction conditions are as follows: 1.0 mmol of fluorene, 1.5 mmol of alcohol, 0.15 mmol of KO^{t}Bu, 1.5 mol% pre-catalyst [**2**] loading in 3.0 mL of toluene solvent at 90 °C for 16 h. It is noteworthy that this optimum temperature is lower than that required for previously reported systems (Table S1). Thus, the complex [**2**] is indeed highly efficient. Notably, we observed that the pre-catalyst is stable up to 202 °C, which was detected by its thermogravimetric analysis (Fig. S1).

With the optimal reaction condition in hand, we explored the versatility of the pre-catalysts with various alcohols and fluorenes. Intrigued by the efficiency of our newly synthesized pre-catalysts, we first examined the reaction of unsubstituted fluorene and benzyl alcohols. Only pre-catalyst [**2**] was explored, as it was more efficient than [**1**]. The desired C9-alkylated products were obtained in excellent yields when fluorene was coupled with benzyl alcohols bearing electron-donating groups at *ortho*, *meta* and *para* positions. For example, methyl-, isopropyl- and *tert*-butyl-substituted benzyl alcohols furnished the corresponding alkylated products **5ab–5af** in 75–89% yield (Scheme 3). Methoxy-substituted benzyl alcohols furnished **5ag–5ai** (Scheme 3) in slightly higher yields (91–93%). Alcohols containing electron-withdrawing group(s), like fluoro, chloro, bromo, di-chloro, CF_3 and di-CF_3, also reacted smoothly with fluorene to afford the desired C9-alkylated products **5aj–5ao** in 70–80% yields (Scheme 3). Biphenyl-substituted alcohol was also effective under this catalytic protocol and furnished the desired product **5ap** in 69% isolated yield (Scheme 3). *N*,*N*-Dimethylbenzyl alcohol was also effective and furnished **5aa′** in 78% yield (Scheme 3).

Next, we sought to explore the scope of the reaction further by employing various substituted fluorenes. Delightfully, di-*tert*-butyl-substituted fluorene derivatives coupled effectively with benzyl alcohols, as well as alcohols bearing electron-donating group(s) at the *ortho*, *meta* and *para* positions, to give the corresponding alkylated products **5ba–5bi** (Scheme 3). Methyl-, isopropyl- and methoxy-substituted benzyl alcohols furnished the desired alkylated fluorenes **5bb–5bi** in 72–82% yield (Scheme 3). Chloro-substituted benzyl alcohol was also found to be very effective with di-*tert*-butyl-substituted fluorene, providing **5bk** in 70% yield (Scheme 3). Next, we tried the reaction of electron-withdrawing mono-bromo-substituted fluorene with benzyl alcohols, and interestingly, we obtained the desired products **5ca–5co** in moderate to excellent yields of 69–80% (Scheme 3). It is noteworthy that reactions of fluorene with 2-nitrobenzyl alcohol, 4-nitrobenzyl alcohol or alcohols

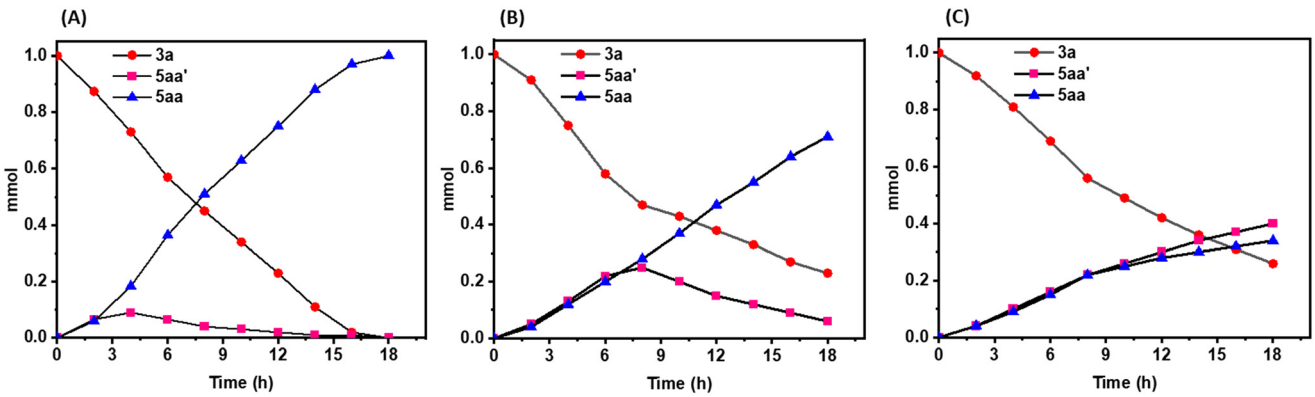

Fig. 1 Reaction kinetic profiles for the C9-alkylation of fluorenes at (A) 90 °C, (B) 75 °C and (C) 60 °C.

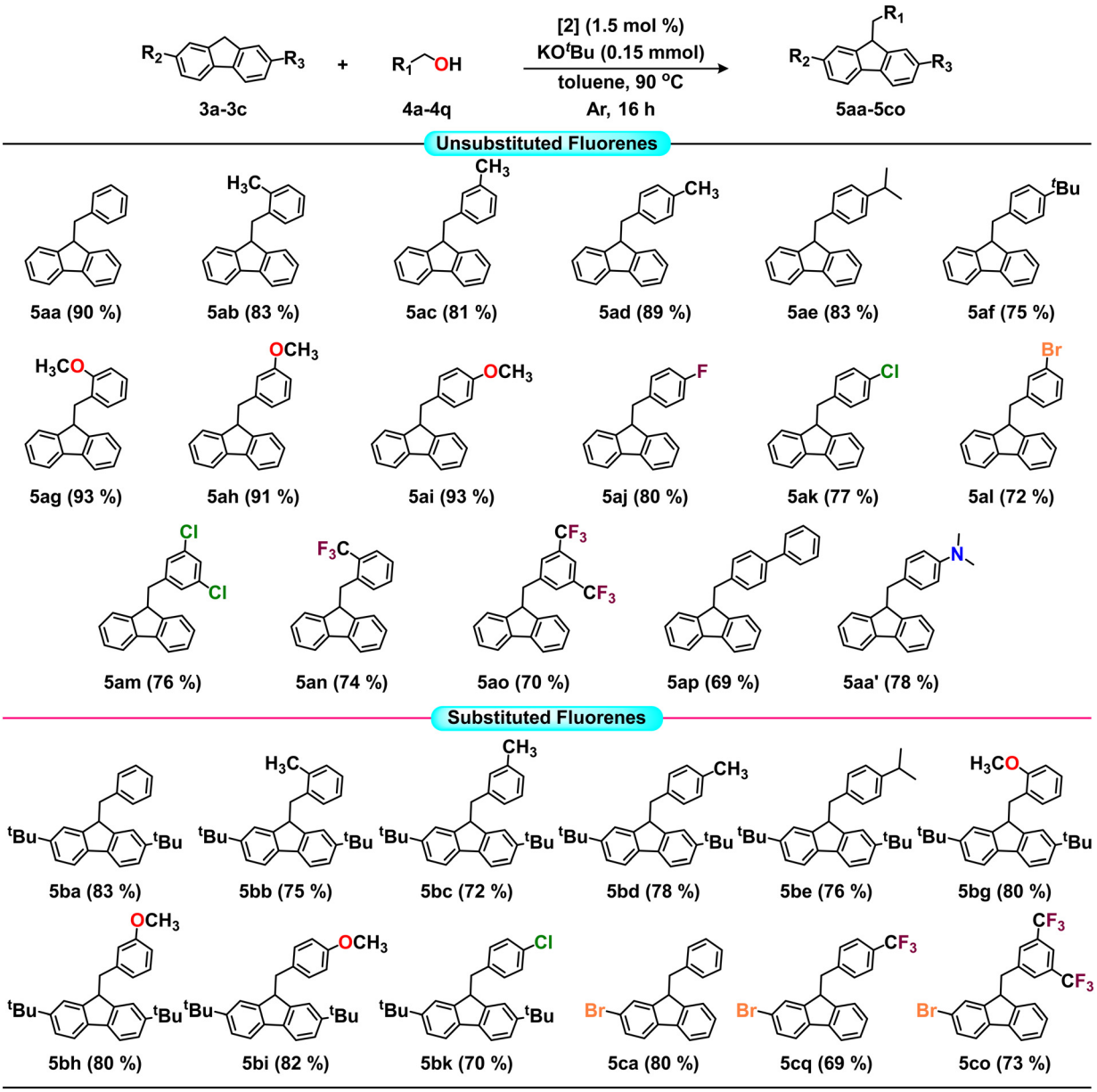

Scheme 3 Substrate scope of fluorenes with a wide array of alcohols. Reaction conditions: [2] (5.81 mg, 1.5 mol%, 0.015 equiv.), fluorene (1.0 mmol, 1.0 equiv.), alcohols (1.50 mmol, 1.5 equiv.), KO^{t}Bu (16.83 mg, 0.15 mmol, 0.15 equiv.), toluene (3.0 mL, 0.33 M), 90 °C (oil bath), and 16 h under argon atmosphere. Yields are reported as isolated yields.

containing protic and/or Lewis-acidic functional groups were not successful under this catalytic protocol. A list of unsuccessful alcohols is mentioned in Scheme S2. When we tried the reaction of indene instead of fluorene, a mixture of products was formed.

It is important to mention here that the developed catalytic protocol was also effective with secondary alcohols, resulting in the C–C coupled products in reasonable yields (Scheme 4). Thus, the reaction of fluorene with secondary alcohols like 1-phenylethan-1-ol, 1-(*p*-tolyl)ethan-1-ol and 1-(4-chlorophenyl)ethan-1-ol resulted in the corresponding products **5ar–5at** in 53–59% yield (Scheme 4). We also explored the C9-alkylation reaction with aliphatic alcohols, and we found that the protocol was indeed effective. Alcohols like ethanol, isopropanol, butanol, and hexanol reacted with unsubstituted fluorene, resulting in the C9-alkylated products **5au–5ax** in 59–68% yield (Scheme 4). Di-*tert*-butyl-substituted fluorene reacted efficiently with ethanol and hexanol, and these resulted in desired alkylated fluorenes **5bu** and **5bw** in 60% and 70% yield, respectively (Scheme 4). Moreover, mono-bromo-substituted fluorene coupled with hexanol to furnish the C9-alkylated product **5cx** in 68% yield (Scheme 4). It should be noted that reactions involving secondary and aliphatic alcohols needed higher base and catalyst loadings, as well as higher temperature, compared to reactions with benzylic alcohols.

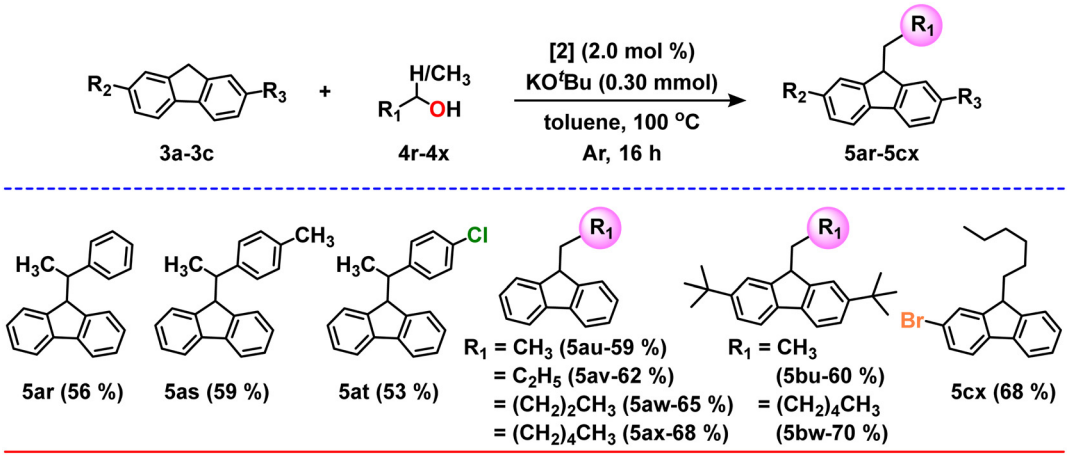

Scheme 4 Substrate scope of the C9-alkylation of fluorenes with secondary and aliphatic alcohols. Reaction conditions: [2] (7.75 mg, 2.0 mol%, 0.02 equiv.), fluorene (1.0 mmol, 1.0 equiv.), alcohols (1.50 mmol, 1.5 equiv.), KO^{t}Bu (33.66 mg, 0.30 mmol, 0.30 equiv.), toluene (3.0 mL, 0.33 M), 100 °C (oil bath), and 16 h under an argon atmosphere. Yields are reported as isolated yields.

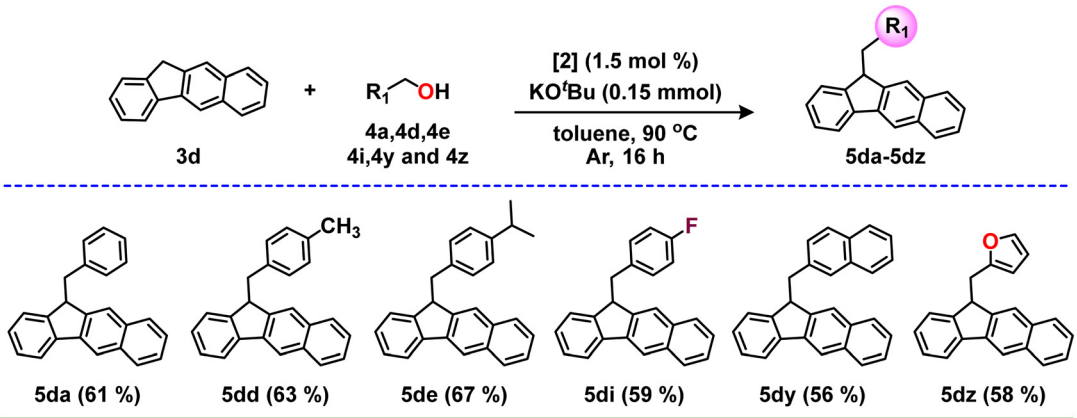

Scheme 5 Substrate scope of extended conjugated 11*H*-benzo[b]fluorenes with benzyl alcohols. Reaction conditions: [2] (5.81 mg, 1.5 mol%, 0.015 equiv.), 11*H*-benzo[*b*]fluorene (216.28 mg, 1.0 mmol, 1.0 equiv.), alcohols (1.50 mmol, 1.5 equiv.), KO^{t}Bu (16.83 mg, 0.15 mmol, 0.15 equiv.), toluene (3.0 mL, 0.33 M), 90 °C (oil bath), and 16 h under an argon atmosphere. Yields are reported as isolated yields.

Encouraged by the efficiency of our catalytic protocol, we turned our attention towards the synthesis of functionalized fluorenes having extended aromatic rings. In these aspects, we attempted the reaction of 11*H*-benzo[*b*]fluorene with benzyl alcohol, which indeed was successful and resulted in the alkylated product **5da** in 61% isolated yield (Scheme 5). Next, we varied the reaction with 4-methylphenyl, 4-isopropylphenyl, 4-fluorophenyl, naphthalene, and furan-derived alcohols, and these were also found to be effective in resulting in the targeted alkylated products **5dd**–**5dz** in good to moderate yields of 56–67% (Scheme 5).

We were further interested in extending the scope and utility of our catalytic protocol for the synthesis of various fluorene analogues (Scheme 6) of the drug benflumetol. First, the reaction of 2-(dibutylamino)-1-(2,7-dichloro-9*H*-fluoren-4-yl)ethan-1-ol and benzyl alcohol under the optimized conditions afforded the desired product **5ea** in 71% yield (Scheme 6). Both electron-donating groups, like methyl, isopropyl, *tert*-butyl and methoxy groups, as well as electron-withdrawing groups, like fluoro-, chloro- and bromo-substituted benzyl alcohols, reacted with 2-(dibutylamino)-1-(2,7-dichloro-9*H*-fluoren-4-yl)ethan-1-ol and afforded the corresponding alkylated products **5eb**–**5el** in 60–80% yields (Scheme 6). The dichloro-substituted alcohols also reacted smoothly with 2-(dibutylamino)-1-(2,7-dichloro-9*H*-fluoren-4-yl)ethan-1-ol and afforded the desired C9-alkylated product **5em** in 60% yield (Scheme 6). Next, reactions between aliphatic alcohols like butanol and hexanol and 2-(dibutylamino)-1-(2,7-dichloro-9*H*-fluoren-4-yl)ethan-1-ol under the optimized conditions produced the desired product **5ew** in 54% and **5ex** in 58% yield (Scheme 6). Thus, our catalytic protocol is indeed versatile and compatible with drug-derived molecules.

It is noteworthy that our catalytic protocol was also found to be effective in gram-scale reactions (Fig. 2). Gram-scale reactions were performed by keeping the amount of KO^{t}Bu and pre-catalyst [2] the same as in the standard catalytic

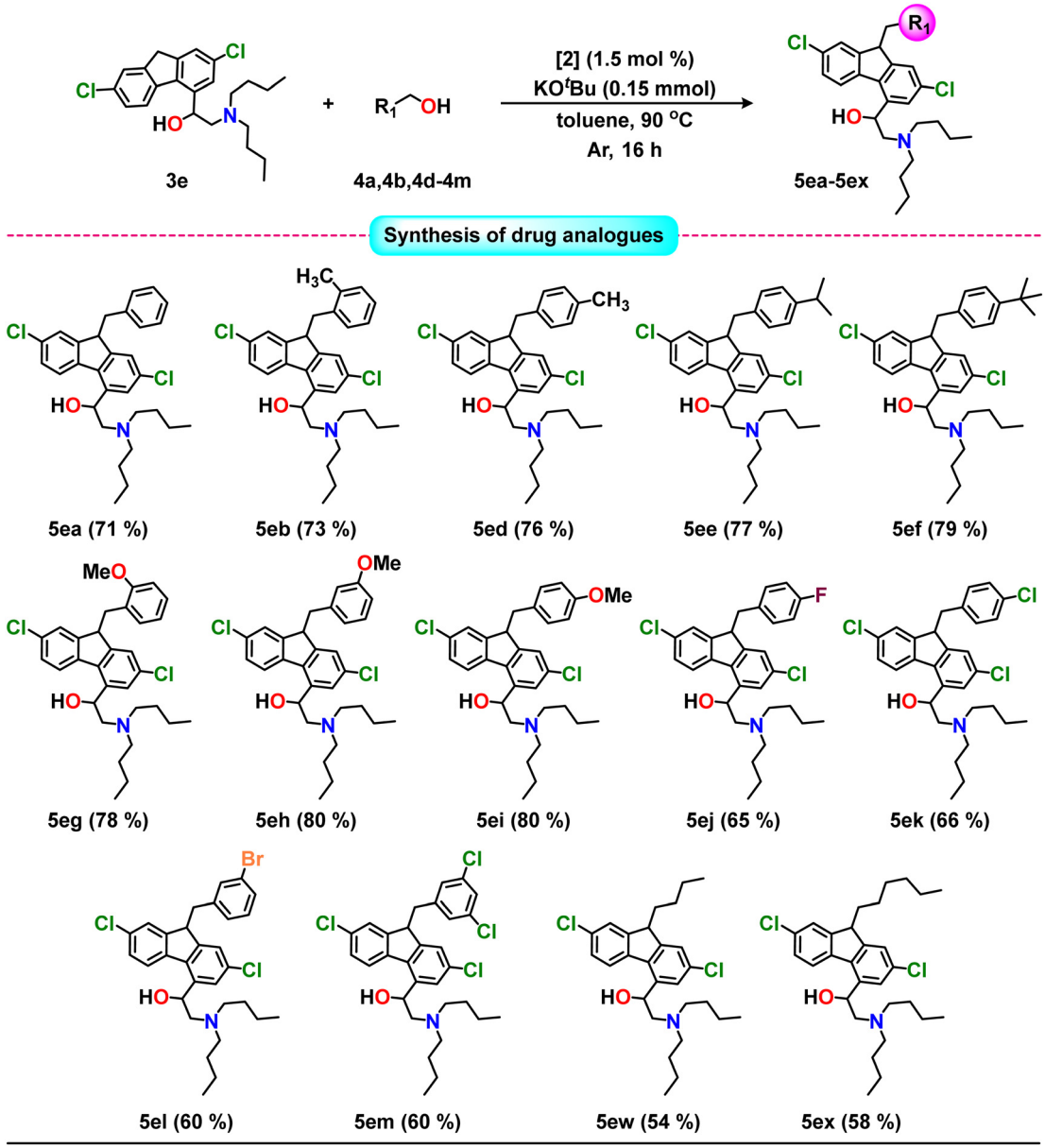

Scheme 6 Substrate scope of 2-(dibutylamino)-1-(2,7-dichloro-9*H*-fluoren-4-yl)ethan-1-ol with a wide array of alcohols. Reaction conditions: [**2**] (5.81 mg, 1.5 mol%, 0.015 equiv.), 2-(dibutylamino)-1-(2,7-dichloro-9*H*-fluoren-4-yl)ethan-1-ol (406.4 mg, 1.0 mmol, 1.0 equiv.), alcohols (1.50 mmol, 1.5 equiv.), KO^{t}Bu (16.83 mg, 0.15 mmol, 0.15 equiv.), toluene (3.0 mL, 0.33 M), 90 °C (oil bath), and 16 h under an argon atmosphere. Yields are reported as isolated yields.

reaction conditions, as well as by increasing the amount of KO^{t}Bu and pre-catalyst [**2**] loadings. The reactions of fluorene (**3a**), 2-(dibutylamino)-1-(2,7 dichloro-9*H*-fluoren-4-yl)ethan-1-ol (**3e**), di-*tert*-butyl fluorene (**3b**) and 11*H*-benzo[*b*]fluorene (**3d**) with benzyl alcohol were used for gram-scale synthesis (Fig. 2). These reactions afforded the respective products in 65–96% yield. It was found that the gram-scale reaction of fluorene (6.02 mmol) with benzyl alcohol, using the same amount of pre-catalyst and base as for the 1.0 mmol of fluorene, resulted in **5aa** in 32% yield (Fig. 2a). Thus, we optimized the pre-catalyst and base loading further. The changes in the yield with different amounts of pre-catalyst loading are shown in Fig. 2a′. It was observed that 1.0 mol% of [**2**] was enough to achieve the highest yield of 96% for **5aa**. With 1.0 mol% of [**2**], **3e** resulted in **5ea** in 65% yield (Fig. 2b). Fluorenes **3b** and **3d** reacted with benzyl alcohol, resulting in the products **5ba** and **5da** in 85% and 68% yields, respectively (Fig. 2c and d). Details of the synthesis are provided in the experimental section and SI (Table S2).

Mechanistic consideration

To have some idea about the mechanism of the reaction, we conducted further studies. The alkylation of fluorene with

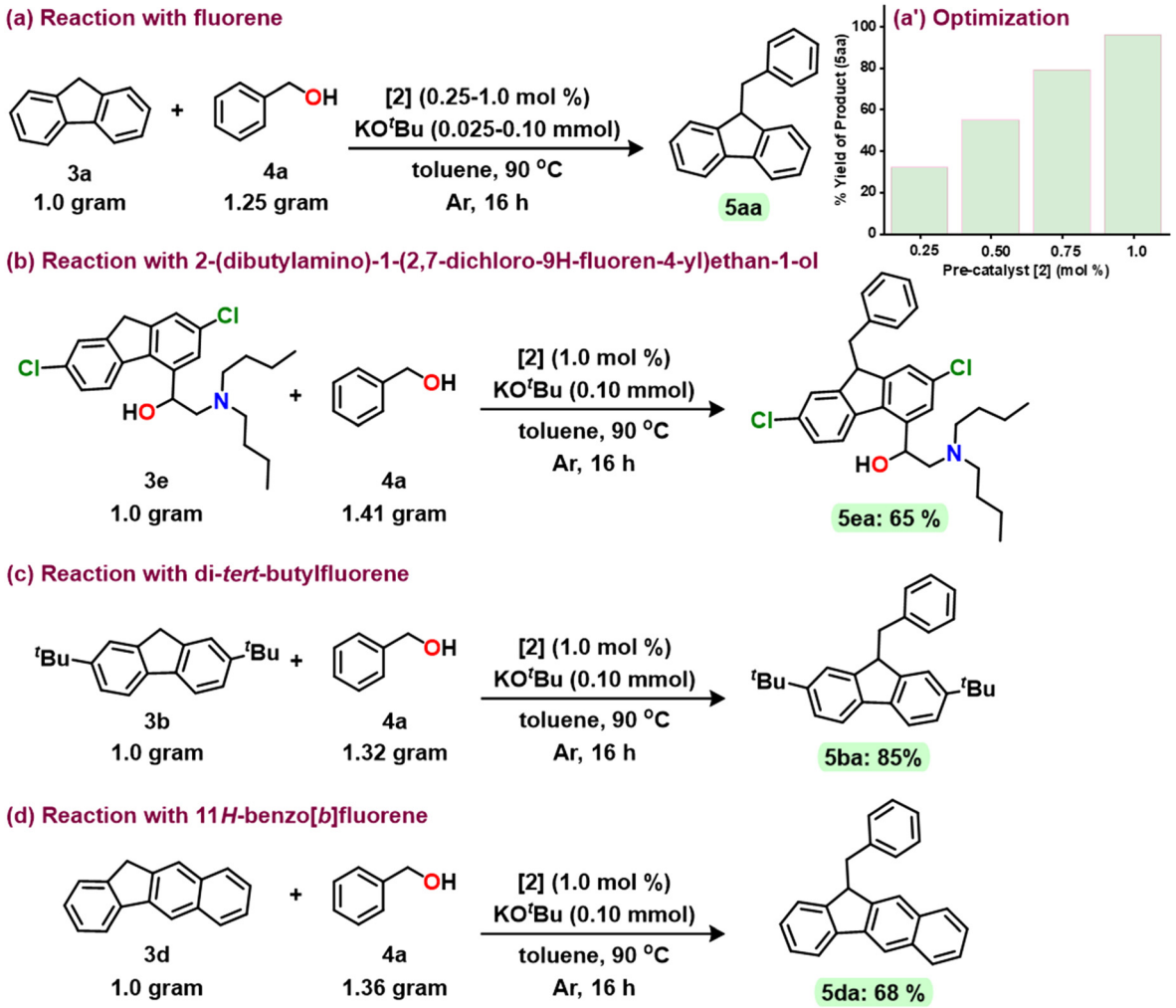

Fig. 2 Gram-scale synthesis.

alcohol generally occurs through three steps:[15b–f,16a–c] (i) first oxidation of alcohol occurs to generate the carbonyl compound; (ii) subsequently, C–C bond formation between the generated carbonyl compound and fluorene to form the alkene intermediate; and (iii) finally, hydrogenation of the alkene intermediate results in the product with the regeneration of the catalyst. Recently, we demonstrated that complex [2], in the presence of KO^{t}Bu, generates the intermediate [2]′, which, in the presence of benzyl alcohol, forms the active catalyst intermediate **A** (Scheme 8).[23] Intermediate **A**, using its ligand-based redox events,[23,27a] generates the carbonyl compound *via* intermediate **B**.[23] To probe this radical pathway, we examined the C9-alkylation of fluorene with benzyl alcohol in the presence of the radical scavenger TEMPO. Indeed, in line with our previous study, we observed a very low yield of the C9-alkylated product **5aa** (Scheme 7A). TEMPO-trapped alcohol was identified *via* HRMS, showing a signature fingerprint at m/z = 301.1426 amu for $[(M + K) - e^-]^+$ (Fig. S127).[12a] In EPR measurements, the reaction mixture always showed a single-line EPR signal characteristic of a ligand-based spin (Fig. S130a).[23] In XPS, we observed the binding energy of Cu 2p electrons characteristic of a Cu(I) complex (Fig. S130b). These results are in line with the alcohol oxidation reaction mediated by [2], as observed by us very recently.[23] Thus, these indicate that the ligand-radical intermediates **A** and **B** are involved in the alcohol oxidation reaction, as shown in Scheme 8. The carbonyl compound generated *via* **B** then undergoes C–C bond formation at the C9 position of deprotonated fluorene, forming intermediate **D** (Scheme 8). Intermediate **D** subsequently undergoes hydrogenation to yield the final product **5aa** *via* intermediate **E**, as shown in Scheme 8.

To probe the intermediates in Scheme 8, we conducted further studies. First, we studied the reaction of fluorene with benzaldehyde, and indeed, we observed the formation of the alkene intermediate **5aa′** as the major product, along with a trace amount of **5aa** (Scheme 7B). To probe the hydrogenation reaction of **5aa′**, we studied the catalytic hydrogenation of **5aa′** in the presence of benzyl alcohol and pre-catalyst [2] (Scheme 7C). The reaction resulted in the C9-alkylated product **5aa** in 79% yield, along with benzaldehyde (Scheme 7C). This indicates that, for the hydrogenation

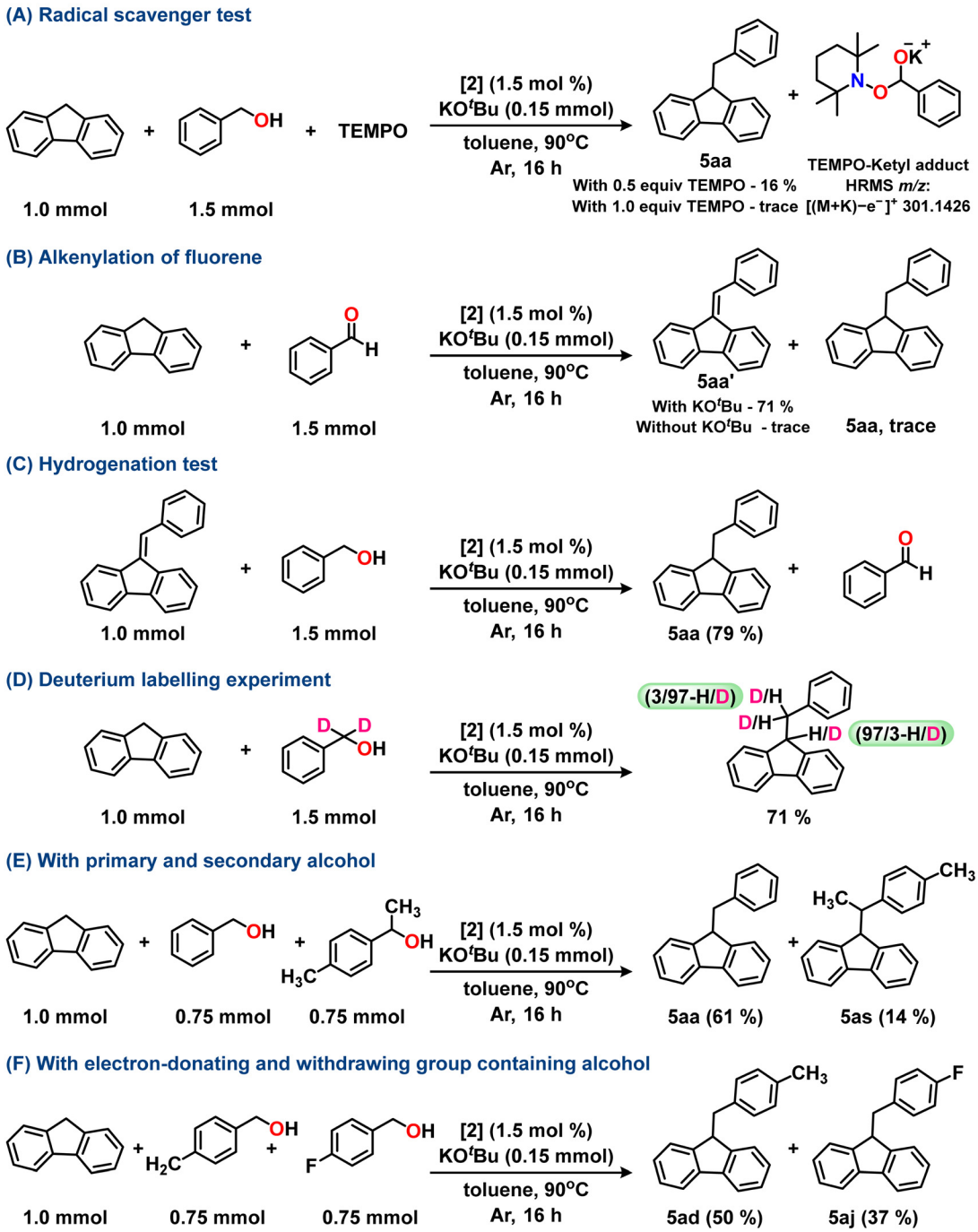

Scheme 7 Control experiments on mechanistic investigation (A–D) and comparative C–C coupling reactions between substituted alcohols (E and F).

reaction, alcohol indeed acts as a source of hydrogen. To probe it further, we studied the reaction in the presence of $PhCD_2OH$. Indeed, we found 97% enrichment of deuterium at the carbon adjacent to the C9 position of fluorene. The C9 carbon has only 3% deuterium (Scheme 7D and Fig. S128 and S129). Thus, it indicates that the alkene intermediate **5aa′**, from the *in situ*-generated carbonyl compound and deprotonated fluorene, forms the new intermediate **D** *via* **C** for the hydrogenation reaction (Scheme 8).[15b,g,16a] The alkene-bound intermediate **D** by the intramolecular transfer of two electron and a proton from the hydrazido motif of the ligand to the alkene generated the intermediate **E**.

The intermediate **E**, upon deprotonation by the incoming alcohol, released the alkylated product **5aa** with the regeneration of the active catalyst **A**. It is noteworthy that such hydrogenation of an alkene intermediate by a reduced azo-ligand has been reported in the literature.[8b,17a] As the catalyst intermediate **D** (Scheme 8) has low-valent Cu(I) and overall, it is electronically

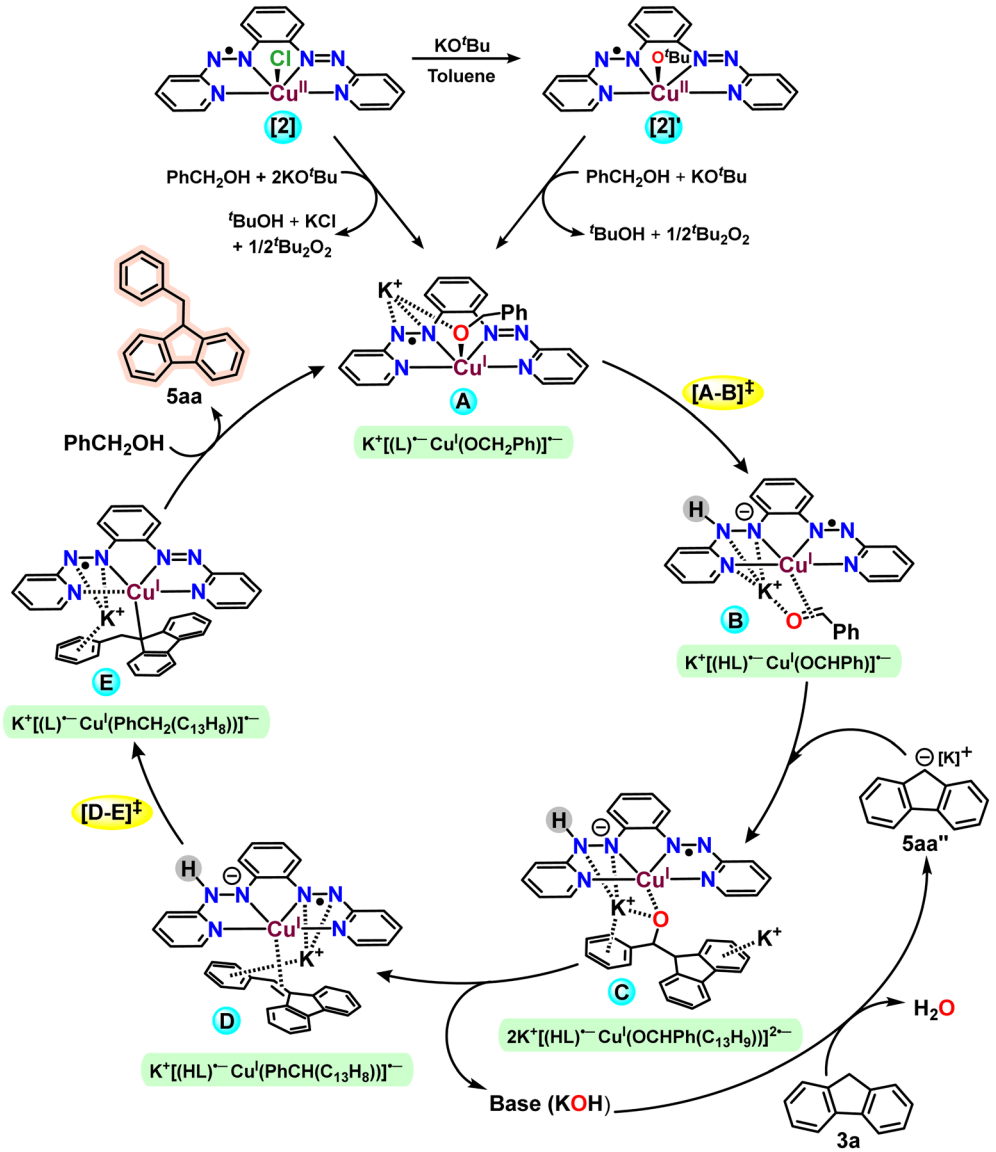

Scheme 8 Plausible reaction mechanism for unsubstituted fluorene and benzyl alcohol (only selected interactions with K^+ are shown for clarity).

very rich, the generally difficult hydrogenation reaction of **5aa′** successfully occurred at a lower temperature.

To evaluate the feasibility of the formation of intermediates, as shown in Scheme 8, we performed DFT calculations as well. It was observed that the formation of the active catalyst **A**, $K^+[(\mathbf{L})^{\bullet-}Cu^I(OCH_2Ph)]^{\bullet-}$, from KO^{t}Bu and benzyl alcohol is quite feasible, and it has ΔG = −8.3 kcal mol^{-1} (Scheme S2). The active catalytic intermediate was optimized with a square-pyramidal geometry at the metal. K^+ remained as a contact ion pair close to the metal-bound alkoxide oxygen and one of the azo moieties (Table S3). The d_{N-N} bond length in **A** was ∼1.346 Å, which is significantly elongated compared to the unreduced azo bond lengths.[28] All Cu–N bond distances were in the range of 1.991–2.059 Å, and the Cu–O bond distance was ∼2.117 Å. Examination of spin density distribution showed that one unpaired spin is distributed on both the metal and the ligand (Table S3). Notably, the chloride analogue of **A**, $[(\mathbf{L})^{\bullet-}Cu^ICl]^{\bullet-}$, exists in equilibrium with its valence tautomer, $[(\mathbf{L})^{2-}Cu^{II}Cl]^{\bullet-}$.[23] Thus, the active catalyst **A** may remain in equilibrium with the tautomeric form **A′**, described as $K^+[(\mathbf{L})^2Cu^{II}(OCH_2Ph)]^{\bullet-}$ (Scheme S3). However, ligand-based EPR signal and previous reports indicate that the ligand-radical Cu(I) species $[(\mathbf{L})^{\bullet-}Cu^I$-$Cl]^{\bullet-}$ is predominant at room temperature. Considering that the catalytic reactions are performed at 90 °C, the five-coordinate complex **A**, $K^+[(\mathbf{L})^{\bullet-}Cu^I(OCH_2Ph)]^{\bullet-}$, is involved in the catalysis. Notably, five-coordinate Cu(I) complexes with π-acceptor imine-based ligands are known in the literature.[12d,29] Next, the β-H atom of the bound alkoxide in **A** was transferred to the coordinated ligand, yielding intermediate **B**, in which the carbonyl compound is weakly bound. The other redox-active azo-pyridine motif in **B** is reduced. The free energy for this transformation is −0.6 kcal mol^{-1}, considering **A** as the reference. Examination of the

bond lengths in **B** showed that one of the d_{N-N} bond lengths is ~1.404 Å, and the other is ~1.345 Å, which are much longer than **A**, indicating successive ligand-based reduction (Scheme 8 and Table S3). Examination of the spin density showed that ~0.875 spin is on the ligand (Table S3). Intermediate **B** can be formed from **A** *via* a transition state [**A–B**]‡, which has a free energy of 26.7 kcal mole^{-1} relative to **A** (Fig. 3). As the reaction proceeds through a radical pathway, as evidenced by the formation of the TEMPO–ketyl intermediate[23] (Scheme 7A) when the reaction is performed in the presence of TEMPO, we considered the calculation for the free energy of the formation of the TEMPO–ketyl adduct and the Cu-complex $\mathbf{A_X}'$, as shown in Scheme S5. The free energy change for this reaction is −6.5 kcal mol^{-1}, and the free energy for the formation of the Cu–TEMPO–ketyl intermediate $\mathbf{A_X}''$ requires only 6.4 kcal mol^{-1}.

Notably, the transformation of the Cu–ketyl radical intermediate **Ax** to the Cu-bound carbonyl intermediate **B** (Scheme S6) involves only an internal electron transfer; thus, intermediate **Ax** (Scheme S6) may be very transient. Intermediate **B** can react with the deprotonated fluorene to generate the new intermediate **C**. The ΔG for the formation of **C** is 9.08 kcal mol^{-1}. The alkoxide motif in **C** remains weakly bound to K^+ and the Cu(I) center. Intermediate **C** can form intermediate **D** upon liberation of KOH. The ΔG for the formation of intermediate **D** is 0.08 kcal mol^{-1}. Intermediate **B** can release the carbonyl compound and be converted to intermediate **C′**. The ΔG for this transformation is −12.9 kcal mol^{-1} (Scheme 8). Subsequently, DFT calculations show that ΔG for the formation of the same intermediate **D** from intermediate **C′** is +12.98 kcal mol^{-1}. The optimized structure of **D** shows that the alkene lies in close proximity to the complex, with a distance of only ~3.989 Å (Table S3). The transformation of intermediate **D** to **E** is found to be uphill by only +7.4 kcal mol^{-1}. Intermediate **E** is optimized in a five-coordination geometry, as shown in Scheme 8 and Fig. 3. Examination of the Cu–N bond distances shows that one of the Cu–N bonds is elongated (~3.264 Å) compared to the other Cu–N bonds (2.054–2.241 Å). The Cu–C bond distance is ~2.079 Å. Intermediate **E** is formed from **D** *via* the transition state [**D–E**]‡, which has ΔG = 28.1 kcal mol^{-1} relative to **A**. The [**D–E**]‡ transition state has the most positive Gibbs free energy. It was found that formation of **D** from **B** *via* intermediate **C** has a $\Delta G^{‡}$ of 28.7 kcal mol^{-1}, whereas this value is quite high, $\Delta G^{‡}$ = 40.9 kcal mol^{-1}, when intermediate **C′** is considered (Fig. 3). Thus, it is quite likely that the intermediate **B**, before the release of PhCHO, undergo C–C bond formation with deprotonated fluorene to form

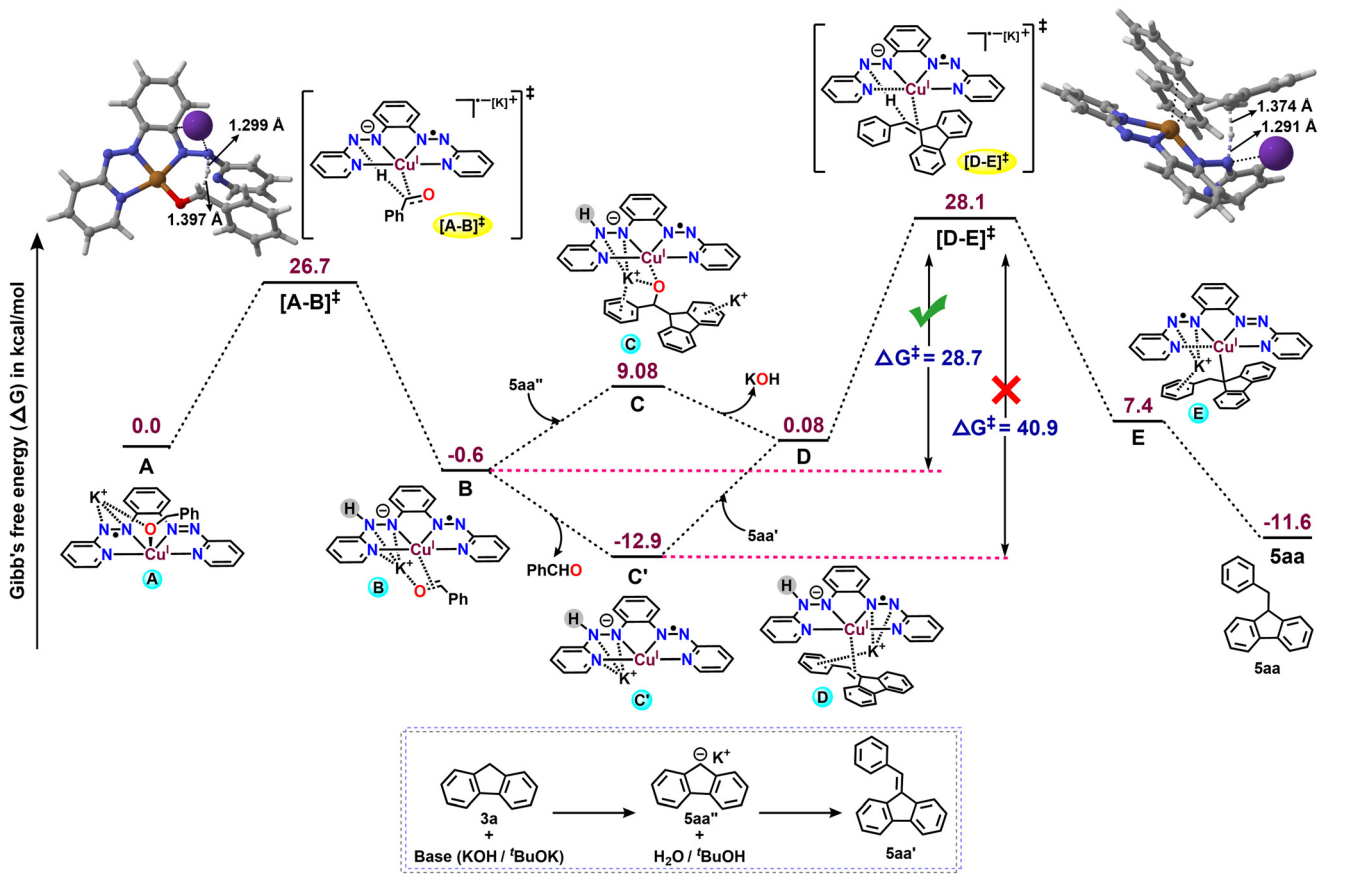

Fig. 3 Gibbs free energy profile (in kcal mol^{-1}) for the formation of 9-benzyl-9*H*-fluorene **5aa** from fluorene **3a** using [A] as the active catalyst (only selected interactions with K^+ are shown for clarity).

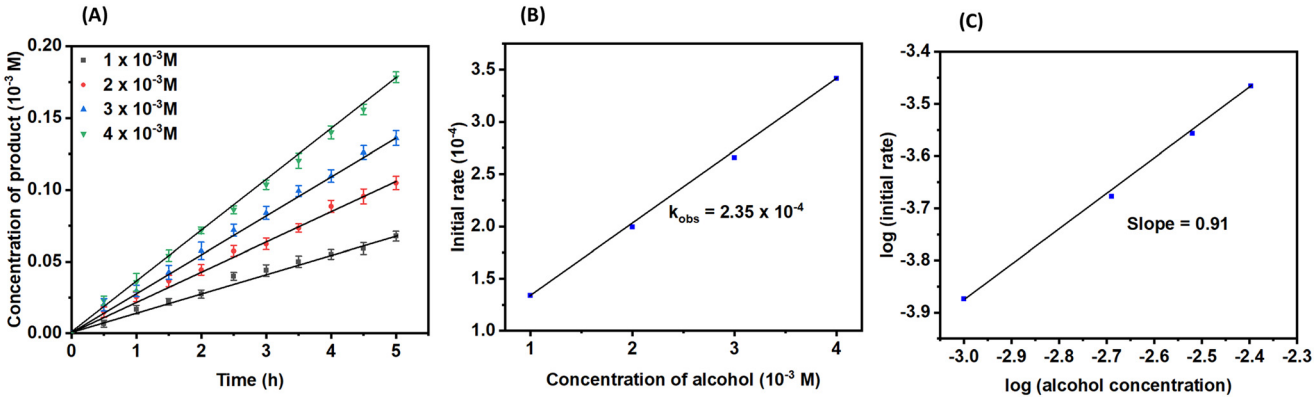

Fig. 4 Kinetic study of benzyl alcohol dehydrogenation at varying alcohol concentrations: (A) product formation over time, (B) initial rate *versus* alcohol concentration and (C) log–log plot showing the reaction order.

intermediate **C**, which, upon release of KOH, generates intermediate **D**. In line with this, we observed that the formation of **5aa′** from fluorene and benzaldehyde proceeds faster when the reaction is performed with [**2**] and base KO^{t}Bu than with base KO^{t}Bu alone (Fig. S131). Intermediate **E** reacts with the incoming alcohol to liberate the alkylated fluorene with the regeneration of the active catalyst **A**. The ΔG for this transformation is −11.6 kcal mol^{-1}. The free energies of all intermediates were calculated relative to **A**, as shown in Fig. 3, and all the optimized structures are provided in the Supporting Information (Table S3). Notably, though the catalytic protocol involves an anionic catalyst, unlike the reaction with hydride transfer pathways, the K^+ counter cation does not directly participate in the dehydrogenation/hydrogenation steps;[30] it remains mainly as a contact ion pair with the active catalyst.

To have further insight into the mechanism, we analyzed the reaction rates for alcohol oxidation using ^{1}H NMR kinetics, as shown in Fig. 4 and 5. Plots of the product concentration *vs.* time were generated using the average of three sets of data. Initial reaction kinetics analysis was performed by varying both the catalyst and alcohol concentrations under pseudo-first-order reaction conditions.[31] Rates of each reaction at different concentrations of alcohol were determined from the slopes of the plots shown in Fig. 4A.[31] A plot of initial rate *vs.* concentration of alcohol showed a linear behavior, with k_{obs} = 2.35 × 10^{-4} (Fig. 4B). The corresponding log (initial rate)–log (alcohol concentration) plot also showed a linear dependence on alcohol concentration, indicating a reaction order of 0.91 with respect to alcohol concentration (Fig. 4C). The analysis of the plot by varying catalyst concentration also showed the linear behavior for the initial rate *vs.* catalyst concentration, with k_{obs} = 1.64 × 10^{-4} (Fig. 5B). The log (initial rate)–log (catalyst concentration) plot showed that the order of the reaction was 0.95 (Fig. 5C). Thus, these observations indicate that both the alcohol and catalyst are involved in the rate-determining step of the alcohol oxidation reaction.

To understand the fate of hydrogenation of **5aa′**, generated from the reaction of fluorene and benzyl alcohol, we studied the hydrogenation of **5aa′** by varying both the catalyst and **5aa′** concentrations. For this, initial ^{1}H NMR kinetics were performed. The rates of each reaction at different concentrations of catalyst were determined from the slopes of each plots shown in Fig. 6A. A plot of initial rate *vs.* concentration of catalyst showed linear behavior, with k_{obs} = 7.42 × 10^{-5} (Fig. 6B). The corresponding log (initial rate)–log (catalyst concentration) plot also showed a linear dependence

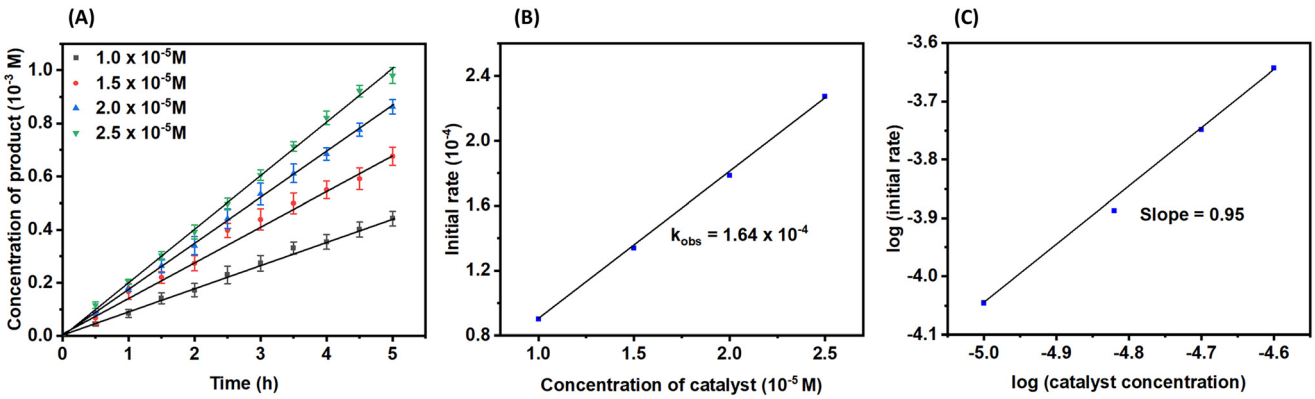

Fig. 5 Kinetic study of benzyl alcohol dehydrogenation at varying catalyst concentrations: (A) product formation over time, (B) initial rate *versus* catalyst concentration and (C) log–log plot showing the reaction order.

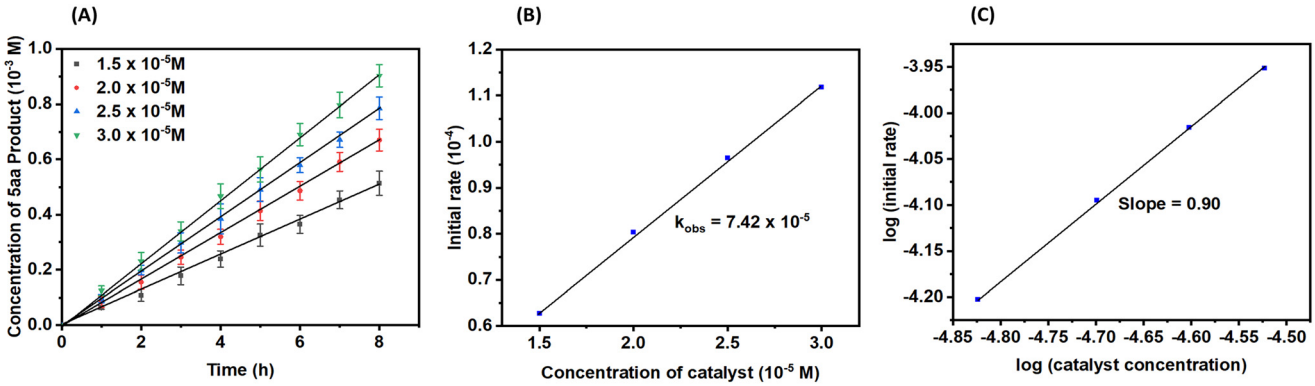

Fig. 6 Kinetics study of **5aa**′ hydrogenation with benzyl alcohol at varying catalyst concentrations: (A) **5aa** product formation over time, (B) initial rate *versus* catalyst concentration and (C) log–log plot showing the reaction order.

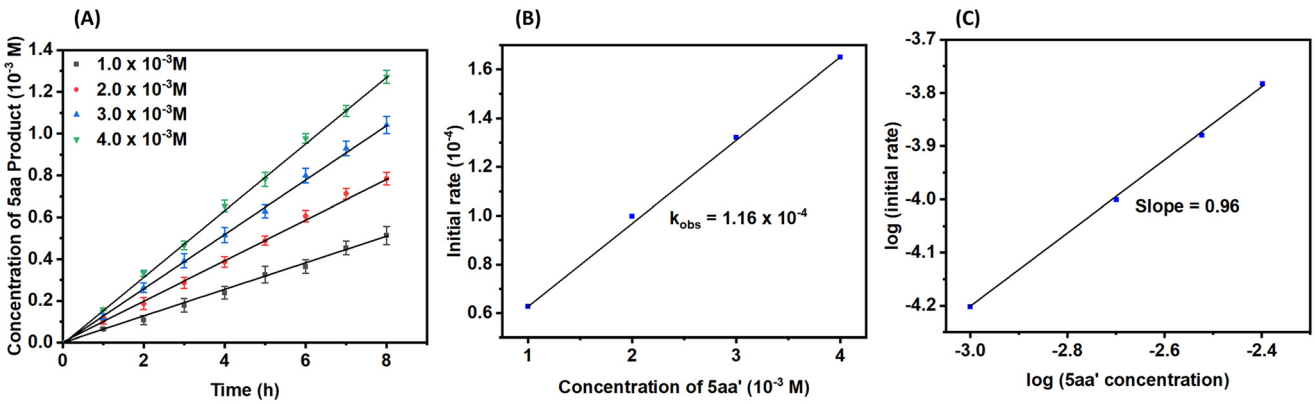

Fig. 7 Kinetic study of **5aa**′ hydrogenation with benzyl alcohol at varying **5aa**′ concentrations: (A) **5aa** product formation over time, (B) initial rate *versus* **5aa**′ concentration and (C) log–log plot showing the reaction order.

on catalyst concentration resulting in a 0.90 order w.r.t. alcohol concentration (Fig. 6C). Analysis of the plot by varying **5aa**′ concentration also showed linear behavior for both the initial rate *vs.* **5aa**′ concentration (Fig. 7B) and their log (initial rate)–log (**5aa**′ concentration) plots (Fig. 7C). In this case, k_{obs} = 1.16 × 10^{-4}, and the order of the reaction with respect to **5aa**′ was 0.96 (Fig. 7B and C). These observations also indicated that both **5aa**′ and catalysts are involved in the rate-determining step of the reaction. However, k_{obs} for **5aa**′ hydrogenation is slightly lower than the k_{obs} for alcohol oxidation, which is in line with the results observed in the time-dependent ^{1}H NMR of the reaction mixture (Fig. 1A).

To evaluate the selectivity of our catalytic protocol, we performed several competitive reactions. A competitive reaction between benzyl alcohol and 1-(*p*-tolyl)ethan-1-ol in an equimolar ratio showed that the primary benzyl alcohol reacts faster than the secondary 1-(*p*-tolyl)ethan-1-ol (Scheme 7E). Another set of competition experiment was also performed between electron-donating 4-methylbenzyl alcohol and electron-withdrawing 4-fluorrobenzyl alcohol, which resulted in **5ad** as the major product (50%) and **5aj** as the minor product (37%), indicating that alcohols with electron-donating groups are more reactive and selective than those with electron-withdrawing groups (Scheme 7F).

Experimental section

Materials

All reagents were of analytical grade purity, commercially available, and used without further purification. Almost all solvents were of reagent and spectroscopic grade and were further purified and dried using standard procedures. All reactions for ligand and complex preparation were carried out under an open atmosphere.

Instrumentation and methods

All synthesized products were isolated and characterized using ^{1}H and ^{13}C{^{1}H} NMR spectroscopies and high-resolution mass spectrometry. ^{1}H, ^{13}C{^{1}H} and ^{19}F NMR spectra were recorded using a 500 MHz JEOL spectrometer, and high-resolution mass spectroscopy (HRMS) was performed on a Waters QTOF mass spectrometer. Chemical shifts are reported as δ-values in parts per million (ppm) relative to tetramethylsilane (TMS) as an internal reference and solvent peaks for ^{1}H NMR and ^{13}C{^{1}H} NMR, respectively. Multiplicities are indicated as s (singlet), d (doublet), t (triplet), dd (doublet of doublet), td (triplet of doublet), ddd (doublet of doublet of doublet), or m (multiplet). Coupling constants (J) are reported in hertz (Hz). EPR spectra were

recorded on a Bruker BiospinEMX^{micro} A-300 spectrometer. XPS data were collected on Nexsa-Thermo Fisher Scientific using an Al Kα X-ray source. Thermogravimetric analysis (TGA) was performed on Perkin Elmer WXT 2500WP.

General procedure for sp^3 C9-alkylation of fluorenes

In a typical reaction, a 10 mL pressure tube was charged in a glove box with alcohols (1.50 mmol, 1.5 equiv.), fluorenes (1.0 mmol, 1.0 equiv.), KO^{t}Bu (16.83 mg, 0.15 mmol, 0.15 equiv.), and pre-catalyst [**2**] (5.81 mg, 1.5 mol%, 0.015 equiv.) in 3.0 mL (0.33 M) of toluene. The reaction mixture was stirred at 90 °C in a pre-heated oil bath for 16 h. Upon completion, the reaction mixture was cooled to room temperature and concentrated *in vacuo*. The residue was purified by column chromatography using hexane : ethyl acetate (99 : 1) as the eluent to afford the pure products. For benflumetol drug analogues, the residue was purified by column chromatography using hexane : ethyl acetate (96 : 4) as the eluent. For reactions with secondary and aliphatic alcohols, KO^{t}Bu (33.66 mg, 0.30 mmol, 0.30 equiv.) and pre-catalyst [**2**] (7.75 mg, 2.0 mol%, 0.02 equiv.) were dissolved in 3.0 mL of toluene (0.33 M) and heated at 100 °C. The desired products were fully characterized by ^{1}H, ^{13}C{^{1}H} and ^{19}F NMR spectroscopy. In addition to NMR, new compounds were characterized using HRMS.

Procedure for gram-scale synthesis of 5aa

In a typical gram-scale reaction, a 30 mL pressure tube was charged in a glove box with [**2**] (5.81 mg, 0.25 mol%, 0.000415 equiv.), KO^{t}Bu (16.83 mg, 0.025 mmol, 0.00415 equiv.), benzyl alcohol (0.976 g, 9.03 mmol, 1.5 equiv.), and fluorene (1.0 g, 6.02 mmol, 1.0 equiv.) dissolved in 15.0 mL (0.40 M) toluene. The reaction mixture was stirred at 90 °C in a pre-heated oil bath for 16 h. Upon completion, the reaction mixture was cooled to room temperature and concentrated *in vacuo*. The residue was purified by column chromatography using hexane : ethyl acetate (99 : 1) as the eluent to afford the pure product (0.494 g, 32%). Detailed optimization studies of pre-catalyst and KO^{t}Bu loadings to achieve the highest yield are given in Table S2 in the SI. The highest yield of **5aa** achieved for gram-scale synthesis was 1.481 g (96%) using [**2**] (23.24 mg, 1.0 mol%, 0.00166 equiv.), KO^{t}Bu (67.32 mg, 0.10 mmol, 0.0166 equiv.), benzyl alcohol (0.976 g, 9.03 mmol, 1.5 equiv.), and fluorene (1.0 g, 6.02 mmol, 1.0 equiv.).

Procedure for gram-scale synthesis of 5ea

In a typical reaction, a 30 mL pressure tube was charged in a glove box with [**2**] (9.53 mg, 1.0 mol%, 0.00465 equiv.), KO^{t}Bu (27.60 mg, 0.10 mmol, 0.04065 equiv.), benzyl alcohol (0.339 g, 3.69 mmol, 1.5 equiv.), and 2-(dibutylamino)-1-(2,7-dichloro-9*H*-fluoren-4-yl)ethan-1-ol (1.0 g, 2.46 mmol, 1.0 equiv.) dissolved in 15.0 mL of toluene (0.16 M). The reaction mixture was stirred at 90 °C in a pre-heated oil bath for 16 h. Upon completion, the reaction mixture was cooled to room temperature and concentrated *in vacuo*. The residue was purified by column chromatography using hexane : ethyl acetate (96 : 4) as the eluent to afford the pure product (0.794 g, 65%).

Procedure for gram-scale synthesis of 5ba

In a typical reaction, a 30 mL pressure tube was charged in a glove box with [**2**] (13.90 mg, 1.0 mol%, 0.002785 equiv.), KO^{t}Bu (40.28 mg, 0.10 mmol, 0.02785 equiv.), benzyl alcohol (0.582 g, 5.39 mmol, 1.5 equiv.), and di-*tert*-butylfluorene (1.0 g, 3.59 mmol, 1.0 equiv.) dissolved in 15.0 mL of toluene (0.24 M). The reaction mixture was stirred at 90 °C in a pre-heated oil bath for 16 h. Upon completion, the reaction mixture was cooled to room temperature and concentrated *in vacuo*. The residue was purified by column chromatography using hexane : ethyl acetate (99 : 1) as the eluent to afford the pure product (1.125 g, 85%).

Procedure for gram-scale synthesis of 5da

In a typical reaction, a 30 mL pressure tube was charged in a glove box with [**2**] (17.89 mg, 1.0 mol%, 0.0021645 equiv.), KO^{t}Bu (51.84 mg, 0.10 mmol, 0.021645 equiv.), benzyl alcohol (0.750 g, 6.94 mmol, 1.5 equiv.), and 11*H*-benzo[*b*]fluorene (1.0 g, 4.62 mmol, 1.0 equiv.) dissolved in 15.0 mL of toluene (0.31 M). The reaction mixture was stirred at 90 °C in a pre-heated oil bath for 16 h. Upon completion, the reaction mixture was cooled to room temperature and concentrated *in vacuo*. The residue was purified by column chromatography using hexane : ethyl acetate (99 : 1) as the eluent to afford the pure product (0.963 g, 68%).

Computational details

All calculations were carried out using density functional theory (DFT) as implemented in the Gaussian16 (revision C.01) suite of package.[32] The M06 hybrid functional[33] was used for geometry optimization of the ligands and complexes using def2-TZVP for Cu atom[34] and the 6-31G(d,p)[35] basis set for all the non-metallic atoms. All the calculations were conducted in the implicit SMD continuum solvation model[36] to capture the solvation effects. Gibbs free energies discussed in the article were computed at the SMD$_{(methanol)}$/M06/6-31G**, def2-TZVP(Cu) level of theory. An isosurface value of 0.004 was used for the visualization of Kohn–Sham molecular orbitals. The 3D images of the optimized geometries were prepared using the CYLView software,[37] and canonical orbitals were rendered using the ChemCraft and GaussView 6.0 software.[38]

Conclusions

In conclusion, using redox, noninnocent N^4-tetradentate bis-azopyridyl ligand containing copper complexes, an efficient sp^3 C–H alkylation of fluorene using alcohols as alkylating agent results in alkylated fluorenes. The redox activity of the ligand in Cu(I) complex played a very crucial role in determining the efficiency of catalytic activities. The catalytic

protocol was versatile, accommodating various fluorenes and benzyl alcohols. It also showed very good functional group tolerance for both alcohols and fluorenes. The catalytic protocol was also efficient for the synthesis of extended conjugated alkylated fluorenes as well as various fluorene analogues of the drug benflumetol. Mechanistic investigations showed that an electronically rich catalyst intermediate was involved over the course of the reaction, enabling successful transformations at lower temperatures. Thus, the present investigation opens up a new avenue of research.

Author contributions

S. H. and Kamal contributed equally to this work.

Conflicts of interest

The authors declare no competing financial interest.

Data availability

The data supporting this article have been included as part of the supplementary information (SI). Supplementary information is available. See DOI: https://doi.org/10.1039/d5cy00956a.

Acknowledgements

SS is thankful to the Science & Engineering Research Board (Grant No. CRG/2023/001476), Government of India, for the financial support. SS also acknowledges IIT Jammu for providing the seed grant support. Kamal acknowledges SERB for providing the fellowship support. SH and AD acknowledges IIT Jammu, and NY acknowledges CSIR for the fellowship support. AC is thankful to the Science & Engineering Research Board (Grant No. CRG/2022/006352), Government of India, for the financial support. SS and AC acknowledge the High-Performance Computing Facility AGASTYA of IIT Jammu. The authors are thankful to the anonymous reviewers for their suggestions at the revision stage to improve the quality of the manuscript.

References

1 (*a*) N. Deibl and R. Kempe, *J. Am. Chem. Soc.*, 2016, **138**, 10786–10789; (*b*) S. Chakraborty, P. Daw, Y. Ben David and D. Milstein, *ACS Catal.*, 2018, **8**, 10300–10305; (*c*) S. Chakraborty, U. K. Das, Y. Ben-David and D. Milstein, *J. Am. Chem. Soc.*, 2017, **139**, 11710–11713.

2 T. Irrgang and R. Kempe, *Chem. Rev.*, 2019, **119**, 2524–2549.

3 (*a*) G. Zhang and S. K. Hanson, *Org. Lett.*, 2013, **15**, 650–653; (*b*) A. J. Rawlings, L. J. Diorazio and M. Wills, *Org. Lett.*, 2015, **17**, 1086–1089.

4 (*a*) S. Rösler, M. Ertl, T. Irrgang and R. Kempe, *Angew. Chem., Int. Ed.*, 2015, **54**, 15046–15050; (*b*) L. Homberg, A. Roller and K. C. Hultzsch, *Org. Lett.*, 2019, **21**, 3142–3147.

5 (*a*) C. Gunanathan and D. Milstein, *Science*, 2013, **341**, 1229712; (*b*) A. J. A. Watson and J. M. J. Williams, *Science*, 2010, **329**, 635–636; (*c*) S. Michlik and R. Kempe, *Nat. Chem.*, 2013, **5**, 140–144; (*d*) S. Budweg, K. Junge and M. Beller, *Catal. Sci. Technol.*, 2020, **10**, 3825–3842.

6 (*a*) K. Barta and P. C. Ford, *Acc. Chem. Res.*, 2014, **47**, 1503–1512; (*b*) R. H. Crabtree, *Chem. Rev.*, 2017, **117**, 9228–9246; (*c*) C. Gunanathan and D. Milstein, *Chem. Rev.*, 2014, **114**, 12024–12087; (*d*) C. Liu, Y. Wei and L. Xie, *Adv. Synth. Catal.*, 2025, **367**, e202401410.

7 (*a*) M. Mastalir, M. Glatz, E. Pittenauer, G. Allmaier and K. Kirchner, *J. Am. Chem. Soc.*, 2016, **138**, 15543–15546; (*b*) K. Das, A. Mondal and D. Srimani, *Chem. Commun.*, 2018, **54**, 10582–10585; (*c*) M. Maji, K. Chakrabarti, B. Paul, B. C. Roy and S. Kundu, *Adv. Synth. Catal.*, 2018, **360**, 722–729.

8 (*a*) S. Elangovan, J.-B. Sortais, M. Beller and C. Darcel, *Angew. Chem., Int. Ed.*, 2015, **54**, 14483–14486; (*b*) S. Bähn, S. Imm, L. Neubert, M. Zhang, H. Neumann and M. Beller, *ChemCatChem*, 2011, **3**, 1853–1864.

9 (*a*) M. H. S. Hamid, P. A. Slatford and J. Williams, *Adv. Synth. Catal.*, 2007, **349**, 1555–1575; (*b*) S. Nandi, I. Borthakur, K. Ganguli and S. Kundu, *Organometallics*, 2023, **42**, 1793–1802.

10 (*a*) R. Sharma, A. Mondal, A. Samanta, N. Biswas, B. Das and D. Srimani, *Adv. Synth. Catal.*, 2022, **364**, 2429–2437; (*b*) A. Mondal, D. Pal, H. J. Phukan, M. Roy, S. Kumar, S. Purkayastha, A. K. Guha and D. Srimani, *ChemSusChem*, 2024, **17**, e202301138.

11 (*a*) S. P. Rath, D. Sengupta, P. Ghosh, R. Bhattacharjee, M. Chakraborty, S. Samanta, A. Datta and S. Goswami, *Inorg. Chem.*, 2018, **57**, 11995–12009; (*b*) R. Pramanick, R. Bhattacharjee, D. Sengupta, A. Datta and S. Goswami, *Inorg. Chem.*, 2018, **57**, 6816–6824; (*c*) D. Sengupta, P. Ghosh, T. Chatterjee, H. Datta, N. D. Paul and S. Goswami, *Inorg. Chem.*, 2014, **53**, 12002–12013.

12 (*a*) B. Goswami, M. Khatua, R. Chatterjee, Kamal and S. Samanta, *Organometallics*, 2023, **42**, 1854–1868; (*b*) M. Khatua, B. Goswami, Kamal and S. Samanta, *Inorg. Chem.*, 2021, **60**, 17537–17554; (*c*) M. Khatua, B. Goswami, A. Devi, Kamal, S. Hans and S. Samanta, *Inorg. Chem.*, 2024, **63**, 9786–9800; (*d*) S. Rani, Kamal, Muskan, A. Changotra and S. Samanta, *Inorg. Chem.*, 2024, **63**, 24517–24531.

13 K. Das, A. Kundu, D. Adhikari and B. Maji, *ACS Catal.*, 2021, **11**, 2786–2794.

14 (*a*) D. Pal, B. Sardar, A. Mondal, K. Mohar, R. Sarmah, H. J. Phukan, R. B. Bera and D. Srimani, *Org. Lett.*, 2025, **27**, 6132–6137; (*b*) S. Hans, M. Adham, M. Khatua and S. Samanta, *J. Org. Chem.*, 2024, **89**, 18090–18108; (*c*) D. Pal, A. Mondal, R. Sarmah and D. Srimani, *Org. Lett.*, 2024, **26**, 514–518.

15 (*a*) M. A. Shaikh, S. G. Agalave, A. S. Ubale and B. Gnanaprakasam, *J. Org. Chem.*, 2020, **85**, 2277–2290; (*b*) A. Mondal, R. Sharma, D. Pal and D. Srimani, *Chem. Commun.*, 2021, **57**, 10363–10366; (*c*) A. Biswas, A. K. Bains and D. Adhikari, *Catal. Sci. Technol.*, 2022, **12**, 4211–4216; (*d*) R. Kumar, S. R. Padhy and E. Balaraman, *J. Org. Chem.*,

2024, **89**, 15103–15116; (*e*) P. Kukreti, R. Chauhan and K. Ghosh, *Catal. Sci. Technol.*, 2025, **15**, 3816–3826; (*f*) S. Naskar, S. Halder, A. Das, S. Malik, G. Kanrar, D. Jana, B. K. Panda, K. Pramanik and S. Ganguly, *Asian J. Org. Chem.*, 2025, e00330; (*g*) A. Samanta, H. J. Phukan, U. K. Tripathi and D. Srimani, *Chem. Commun.*, 2025, **61**, 12582–12585.

16 (*a*) R. Sharma, A. Mondal, A. Samanta and D. Srimani, *Catal. Sci. Technol.*, 2023, **13**, 611–617; (*b*) Kamal and S. Samanta, *J. Org. Chem.*, 2024, **89**, 1910–1926; (*c*) R. Saha, S. K. Maharana, N. Ch. Jana and B. Bagh, *Chem. Commun.*, 2024, **60**, 10144–10147; (*d*) R. Saha, B. C. Hembram, S. Panda, R. Ghosh and B. Bagh, *J. Org. Chem.*, 2024, **89**, 16223–16241; (*e*) S. Pal, A. K. Guin, S. Chakraborty and N. D. Paul, *ChemCatChem*, 2024, **16**, e202400026; (*f*) S. Sahoo, S. Manna and A. Rit, *Chem. Sci.*, 2024, **15**, 5238–5247; (*g*) R. Saha, B. C. Hembram, A. Panda and B. Bagh, *Org. Biomol. Chem.*, 2025, **23**, 4232–4239.

17 (*a*) C. E. Elwell, N. L. Gagnon, B. D. Neisen, D. Dhar, A. D. Spaeth, G. M. Yee and W. B. Tolman, *Chem. Rev.*, 2017, **117**, 2059–2107; (*b*) S.-J. Chen, S. W. Krska and S. S. Stahl, *Acc. Chem. Res.*, 2023, **56**, 3604–3615; (*c*) B. D. Bruin, E. Bill, E. Bothe, T. Weyhermüller and K. Wieghardt, *Inorg. Chem.*, 2000, **39**, 2936–2947.

18 (*a*) R. Schneider, T. A. Engesser, C. Näther, I. Krossing and F. Tuczek, *Angew. Chem., Int. Ed.*, 2022, **61**, e202202562; (*b*) J. D. Tovar, R. Leblay, Y. Wang, L. Wojcik, A. T. Pourret, M. Réglier, A. J. Simaan, N. L. Poul and C. Belle, *Chem. Sci.*, 2024, **15**, 10308–10349.

19 (*a*) B. T. Op't Holt, M. A. Vance, L. M. Mirica, D. E. Heppner, T. D. P. Stack and E. I. Solomon, *J. Am. Chem. Soc.*, 2009, **131**, 6421–6438; (*b*) L. M. Mirica, D. J. Rudd, M. A. Vance, E. I. Solomon, K. O. Hodgson, B. Hedman and T. D. P. Stack, *J. Am. Chem. Soc.*, 2006, **128**, 2654–2665; (*c*) L. M. Mirica, M. Vance, D. J. Rudd, B. Hedman, K. O. Hodgson, E. I. Solomon and T. D. P. Stack, *Science*, 2005, **308**, 1890–1892.

20 (*a*) B. L. Ryland and S. S. Stahl, *Angew. Chem., Int. Ed.*, 2014, **53**, 8824–8838; (*b*) B. L. Ryland, S. D. McCann, T. C. Brunold and S. S. Stahl, *J. Am. Chem. Soc.*, 2014, **136**, 12166–12173.

21 (*a*) J. E. Steves and S. S. Stahl, *J. Am. Chem. Soc.*, 2013, **135**, 15742–15745; (*b*) S. D. McCann and S. S. Stahl, *J. Am. Chem. Soc.*, 2016, **138**, 199–206.

22 (*a*) A. Hoffmann, C. Citek, S. Binder, A. Goos, M. Rübhausen, O. Troeppner, I. Ivanović-Burmazović, E. C. Wasinger, T. D. P. Stack and S. Herres-Pawlis, *Angew. Chem., Int. Ed.*, 2013, **52**, 5398–5401; (*b*) C. Citek, C. T. Lyons, E. C. Wasinger and T. D. P. Stack, *Nat. Chem.*, 2012, **4**, 317–322.

23 S. Hans, Kamal, A. Devi, M. Adham, Muskan, S. Ranaut, A. Changotra, S. Mazumder and S. Samanta, *Inorg. Chem.*, 2025, **64**, 7930–7944.

24 (*a*) K. R. Justin Thomas and A. Baheti, *Mater. Technol.*, 2013, **28**, 71–87; (*b*) S. Liu, K. Zhang, J. Lu, J. Zhang, H.-L. Yip, F. Huang and Y. Cao, *J. Am. Chem. Soc.*, 2013, **135**, 15326–15329.

25 (*a*) A. C. Grimsdale, K. L. Chan, R. E. Martin, P. G. Jokisz and A. B. Holmes, *Chem. Rev.*, 2009, **109**, 897–1091; (*b*) S. W. Thomas, G. D. Joly and T. M. Swager, *Chem. Rev.*, 2007, **107**, 1339–1386.

26 D. T. Chase, A. G. Fix, S. J. Kang, B. D. Rose, C. D. Weber, Y. Zhong, L. N. Zakharov, M. C. Lonergan, C. Nuckolls and M. M. Haley, *J. Am. Chem. Soc.*, 2012, **134**, 10349–10352.

27 (*a*) M. Khatua, B. Goswami, S. Hans, Kamal, S. Mazumder and S. Samanta, *Inorg. Chem.*, 2022, **61**, 17777–17789; (*b*) S. Hans, Kamal, A. Devi, R. Chatterjee, M. Khatua and S. Samanta, *ChemistrySelect*, 2025, **10**, e202501498.

28 (*a*) S. Samanta, P. Ghosh and S. Goswami, *Dalton Trans.*, 2012, **41**, 2213; (*b*) S. Samanta, P. Singh, J. Fiedler, S. Záliš, W. Kaim and S. Goswami, *Inorg. Chem.*, 2008, **47**, 1625–1633; (*c*) B. Goswami, M. Khatua, A. Devi, S. Hans, R. Chatterjee and S. Samanta, *Dalton Trans.*, 2024, **53**, 10250–10260.

29 G. C. Paul, K. Das, S. Maity, S. Begum, H. K. Srivastava and C. Mukherjee, *Inorg. Chem.*, 2019, **58**, 1782–1793.

30 P. A. Dub, *Eur. J. Inorg. Chem.*, 2021, 4884–4889.

31 (*a*) D. R. Williams, A. A. Shah, S. Mazumder and M.-H. Baik, *Chem. Sci.*, 2013, **4**, 238–247; (*b*) P. G. Nandi, P. Maity and A. Kumar, *ACS Catal.*, 2025, **15**, 543–556; (*c*) A. Bisarya, R. V. Jasra and A. Kumar, *Organometallics*, 2023, **42**, 1818–1831.

32 M. J. Frisch, G. W. Trucks, H. B. Schlegel, G. E. Scuseria, M. A. Robb, J. R. Cheeseman, G. B. V. Scalmani, B. Mennucci, G. A. Petersson and H. Nakatsuji, *Gaussian 16, Revision C.01*, Gaussian, Inc., 2019.

33 (*a*) M. Walker, A. J. A. Harvey, A. Sen and C. E. H. Dessent, *J. Phys. Chem. A*, 2013, **117**, 12590–12600; (*b*) Y. Wang, P. Verma, X. Jin, D. G. Truhlar and X. He, *Proc. Natl. Acad. Sci. U. S. A.*, 2018, **115**, 10257–10262; (*c*) Y. Zhao and D. G. Truhlar, *Theor. Chem. Acc.*, 2008, **120**, 215–241.

34 Y. Liu, S. G. Resch, H. Chen, S. Dechert, S. Demeshko, E. Bill, S. Ye and F. Meyer, *Angew. Chem., Int. Ed.*, 2023, **62**, e202215840.

35 (*a*) P. C. Hariharan and J. A. Pople, *Theor. Chim. Acta*, 1973, **28**, 213–222; (*b*) M. M. Francl, W. J. Pietro, W. J. Hehre, J. S. Binkley, M. S. Gordon, J. A. Pople and D. J. DeFrees, *J. Chem. Phys.*, 1982, **77**, 3654–3665.

36 (*a*) A. V. Marenich, C. J. Cramer and D. G. Truhlar, *J. Phys. Chem. B*, 2009, **113**, 6378–6396; (*b*) R. Seeger and J. A. Pople, *J. Chem. Phys.*, 1977, **66**, 3045–3050.

37 C. Y. Legault, *CYLview, 1 0.*, Universitede Sherbrooke, 2009, http://www.cylview.org.

38 (*a*) G. A. Zhurko and D. A. Zhurko, http://www.chemcraftprog.com; (*b*) A. Todd and M. Millam John, *GaussView, Version 6*, Semichem Inc, 2016.